Particle & Particle Systems Characterization
www.particle-journal.com

Core–Shell Poly (Ionic Liquid)@Mesoporous Silica Chemiluminescent Nanoprobes for Sensitive Intracellular Hydrogen Peroxide Imaging

Kai Zhou, Feng Zhang, Jing Xu, Hui He, Weili Wei, and Zhining Xia**

Despite significant developments in spatial distribution imaging of H_2O_2 as one the most important nonradical reactive oxygen species, novel background-free, highly sensitive, and selective probes that allow intracellular sensing are still imperative. This is mainly because the fluorescent probes usually suffer some drawbacks such as, fluorescence bleaching and requirement of bulky light sources. In this study, the rational design and fabrication of a nonenzymatic nanoprobe (c-PIL@mSiO_2) with dramatically improved sensitivity for chemiluminescent (CL) imaging of intracellular and in vivo H_2O_2 at nano molar level is presented. The limit of detection is lower than the endogenous H_2O_2 concentration, and is significantly better than that of some recently reported fluorescent and CL probes. Structurally, the nanoprobe is composed of a unique amphiphilic poly(ionic liquid) core for preserving H_2O_2 responsive reagents, and a mesoporous silica shell acts as an "exoskeleton" to provide hydrophilic nature. The multiple alternating hydrophobic and hydrophilic nanodomains of the poly(ionic liquid) core increase mass transfer dynamics, which increase the sensitivity of H_2O_2 imaging. RAW264.7 macrophages and mice models of inflammations experiment show that the c-PIL@mSiO_2 is capable of imaging H_2O_2 intracellular and in vivo. This probe for the first time achieves CL detection of endogenous intracellular H_2O_2 without disruption of cells.

1. Introduction

Reactive oxygen species (ROS) play numerous biological effects covering a wide spectrum that ranges from physiological regulatory functions to damaging alterations participating in the pathogenesis of increasing number of diseases.[1] Noteworthily, the hydrogen peroxide (H_2O_2) is one of the primary nonradical ROS, and closely relate to many other ROS generated intracellularly.[2] Consequently, highly sensitive and specific detection of H_2O_2 level both extra- and intracellular has receiving broad attention not only for fundamental studies to understand its role in cellular processes but also for early diagnosis.[3] Optical probes that are specific; sensitive; easy to load into organelles, cells, or tissues without subsequent leakage or unwanted diffusion, excretion, or metabolism should be ideal for H_2O_2 detection and spatial distribution visualization.[4] Currently, many molecular[5] and nanoscale[6] fluorescent probes for H_2O_2 have been reported. However, the fluorescent probes usually suffer from some common drawbacks such as requirement of light source, background interference from biomatrices, and fluorescence bleaching.[7] Therefore, novel visualizing strategies that offer ultrahigh sensitivity and intracellular sensing are still imperative.

Luminescent H_2O_2 probes including the enzyme-dependent (i.e., luciferase) bioluminescent probes and nonenzymatic chemiluminescent (CL) probes should be better alternatives to the fluorescent ones. However, bioluminescent detection of H_2O_2 mostly achieved with transgenetic animals or cell expressed with luciferase.[8] This is unfavorable because transgenetic animals are not cost-effective and readily available. Interestingly, many CL systems emit light with the oxidation of H_2O_2. Among them, the peroxyoxalate CL (PO-CL) system responses highly selective to H_2O_2 over other ROS with almost the highest luminescent quantum yield (QY).[9] However, the PO-CL reagents cannot be used directly in biological systems because they are hydrophobic and unstable under aqueous conditions. To resolve this, two strategies have generally been employed. One is to use PO-CL reagents with considerable stability but low luminescent QY, such as oxalates without electron-attracting substituents on the benzene ring.[10] The other is to load PO-CL reagents with high luminescent QY in hydrophobic microcontainers such as micelles.[11] These approaches achieved imaging of H_2O_2 in vivo. However, they precluded detection of intracellular H_2O_2 due in part to insufficient sensitivity and lack of transmembrane ability of these CL probes.[11,12] Hence, a CL probe for intracellular H_2O_2 must have following

Dr. K. Zhou
Analytical and Testing Center
Chongqing University
Chongqing 401331, P. R. China
Dr. F. Zhang, Dr. J. Xu, H. He, Prof. W. Wei, Prof. Z. Xia
School of Pharmaceutical Sciences and Innovative Drug Research Center
Chongqing Key Laboratory of Total Synthesis of Natural Products and Innovative Drug Research
Chongqing University
Chongqing 401331, P. R. China
E-mail: wlwei@cqu.edu.cn; znxia@cqu.edu.cn
The ORCID identification number(s) for the author(s) of this article can be found under https://doi.org/10.1002/ppsc.201700329.

DOI: 10.1002/ppsc.201700329

properties: (1) compatible with the aqueous physiological medium, (2) cell permeable, (3) highly selective and sensitive to H_2O_2 over other biologically relevant ROS.[13] Recently, a novel material, poly (ionic liquids) nanoparticles (PIL) attracted considerable attention, because they combine some unique characters of ionic liquids with the common properties of polymers, such as amphiphilicity, durability, mechanical stability, and the PIL were most likely setup in organized mesophases made up from separated hydrophobic and hydrophilic domains.[14] These special properties bring us inspirations using PIL as a hydrophobic nanocontainer for PO-CL reagents to construct a both in vivo and intracellular H_2O_2 CL probe.

Herein, we designed a core–shell structured nanocontainer (PIL@mSiO_2) that composed of a PIL core and a hydrophilic mesoporous silica shell (**Scheme 1**). The hydrophobic PO-CL reagents including bis[3,4,6-trichloro-2-(pentyloxycarbonyl) phenyl] oxalate (CPPO) and fluorescent dyes (i.e., rubrene) could be preserved in the hydrophobic domains of the PIL core of PIL@mSiO_2. The hydrophilic mesoporous silica shell of the nanoprobe allow for the prompt accessibility of H_2O_2 to the PO-CL reagents that reserved in the hydrophobic PIL core. Subsequently, H_2O_2 can sensitively triggers a PO-CL reaction, i.e., oxidation of peroxalates to form 1,2-dioxetanedione that can transfer its high energy to nearby fluorescent molecules to emit CL.[11] Thus, after the PIL@mSiO_2 was loaded with PO-CL reagents, it should be a CL nanoprobe namely c-PIL@mSiO_2, for H_2O_2. The multiple alternating hydrophobic and hydrophilic nanostructure of the PIL core increased mass transfer dynamics of micro-environmental H_2O_2 to PO-CL reagents.[14b] The mesoporous silica shell acted as an "exoskeleton" which provided high mechanical/chemical stability and hydrophilicity to the nanoprobe. The CL dynamics of c-PIL@mSiO_2 toward H_2O_2 was investigated, and the probe was found to be cell permeable allowing selective and ultrasensitive intracellular and in vivo H_2O_2 imaging.

2. Results and Discussion

The PILs were prepared via a single-step precipitation polymerization as described previously (details see as Supporting Information).[15] The transmission electron microscopy (TEM) image of PILs showed they had an average diameter of about 65 nm (**Figure 1**a), and were well-dispersible in water due to the preferential organization of the charged ionic backbone on the outer surface. During polymerization of 3-*n*-tetradecyl-1-vinylimidazolium dicyanamide, the polymers can spontaneously self-assemble into onionlike multilamellar vesicular nanostructures.[14] In our case, the mole fractions of crosslinking agent was 10%, which formed hydrophilic channels (the charged polymer backbone part) among the hydrophobic domain (the long alkyl side chain part) of the PIL. When the two component PO-CL reagents (CPPO and rubrene) were loaded in the hydrophobic domain of the PIL, the CPPO can react with external

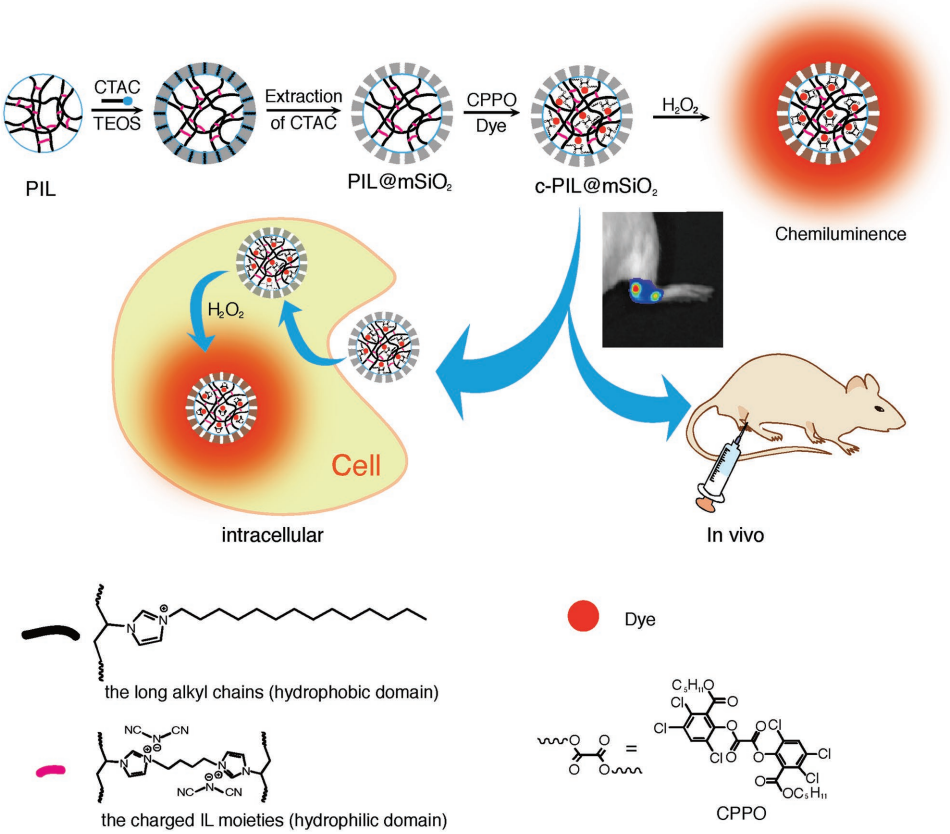

Scheme 1. Schematic illustration of the synthetic route to the PIL@mSiO_2 nanocomposite and application for intracellular and in vivo H_2O_2 imaging.

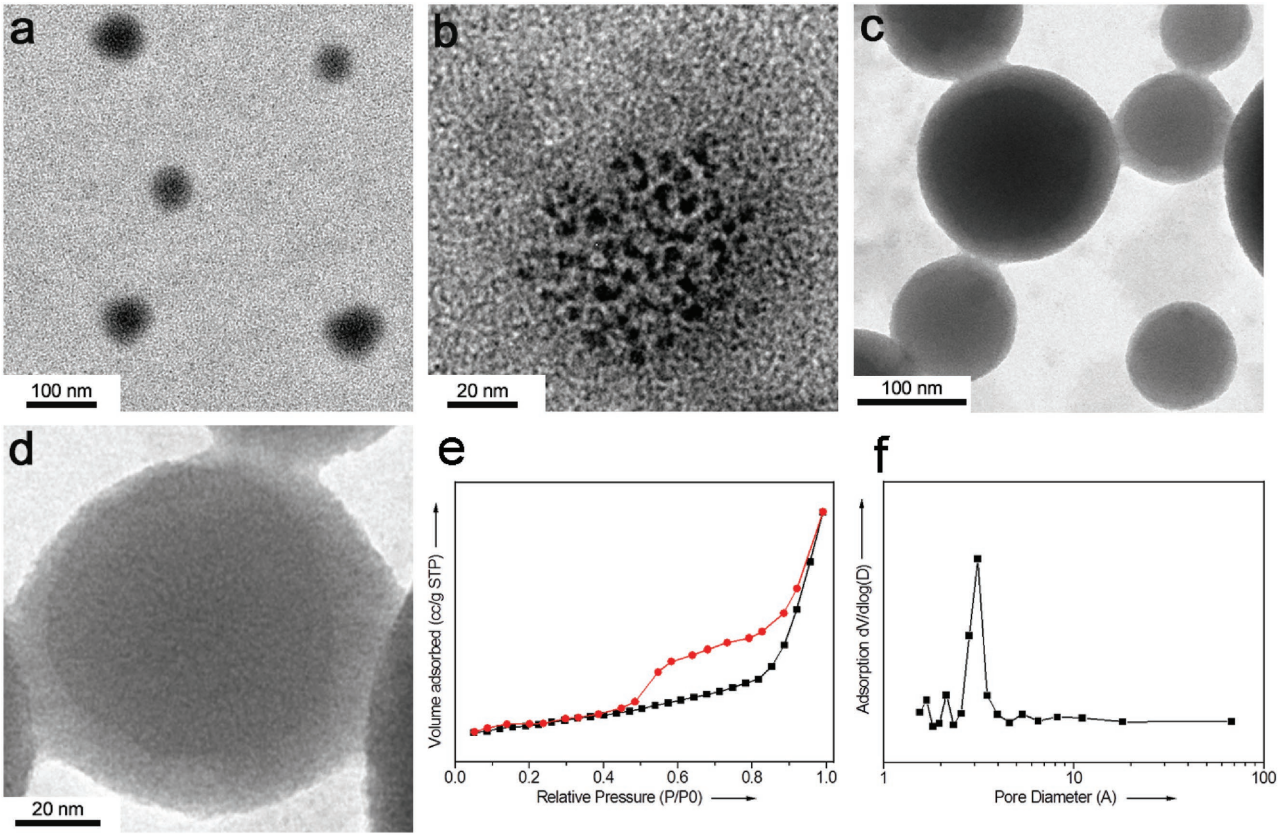

Figure 1. TEM image of PIL nanospheres a,b) and PIL@mSiO$_2$ nanoparticles c,d). Nitrogen adsorption isotherm e), and the BJH pore size f) distribution of PIL@mSiO$_2$ nanoparticles.

H_2O_2 from the aqueous environment efficiently due to the large contact area and self-adaptive ability between the hydrophobic and hydrophilic domains (Figure 1b).[14] This structure is benificial to the detection sensitivity to H_2O_2 comparing other CL nanoprobes.[11] However, as shown in Figure S1a in the Supporting Information, PILs became undispersable in phosphate buffered saline (PBS) after loaded with PO-CL reagents. The PO-CL reagents loaded PILs were named as c-PILs.

Thus the PILs were then coated by a thin hydrophilic shell of mesoporous silica (PIL@mSiO$_2$) according to a previous method with some modification by replacing the surfactant as *N*-hexadecyltrimethylammonium chloride (CTAC).[16] As a result, the PO-CL reagents loaded c-PIL@mSiO$_2$ kept well-dispersed in PBS for weeks (Figure S1b, Supporting Information). Dynamic light scattering (DLS) revealed that the PIL@mSiO$_2$ have an average hydrodynamic diameter of ≈100 nm, suitable for clinical and diagnostic applications (Figure S2, Supporting Information). The TEM image of PIL@mSiO$_2$ clearly indicated a 65 nm PIL core and a silica shell with 10–20 nm thickness (Figure 1c,d). The overall outer diameter is ≈100 nm. This result is consistent with the DLS characterization. The hump at 22 on X-ray diffraction (XRD) pattern (Figure S3, Supporting Information) proves the existence of mesoporous silica shell.[17] The adsorption–desorption isotherm obtained on PIL@mSiO$_2$ shows a type IV behavior with a capillary condensation in the relative pressure range of 0.5–0.9 (Figure 1e), indicating the presence of a porosity organization. The Barrett–Joyner–Halenda (BJH) pore size distribution shows a peak (Figure 1f) corresponding to the mesopores of the shell (3 nm). In addition, the Brunauer–Emmett–Teller (BET) specific surface area and total pore volume are calculated to be 135.2 $m^2\ g^{-1}$ and 0.22 $cm^3\ g^{-1}$, respectively. The shell porosity is crucial for the PIL@mSiO$_2$ to load PO-CL reagents and make the H_2O_2 accessible to them.

The highly efficent PO-CL reagents, CPPO and rubrene, were applied in our work for the purpose of the best detection sensitivity.[18] Both CPPO and rubrene are hydrophobic. According to a previous report,[14a] hydrophobic compounds could be readily loaded into the PIL core of the PIL@mSiO$_2$ nanoparticles via hydrophobic interactions. Herein, the loading of PO-CL reagents into PIL@mSiO$_2$ was proven by thermogravimetric analysis (TGA) and Fourier transform infrared spectroscopy (FTIR). The characteristic peaks (1723, 1568 and 1305 cm^{-1}) in FTIR spectrum of c-PIL@mSiO$_2$ confirmed the succesfull loading of PO-CL reagents (Figure S4, Supporting Information). According to TGA analysis, mass percent of PO-CL reagents in c-PIL@mSiO$_2$ was 14.3% (Figure S5, Supporting Information), and consequently the loading efficiency was 22.8%. This loading capacity is surfficient for continuous H_2O_2 in vivo imaging. In comparison, we also investigated the loading capability of mesoporous silica nanoparticles (with average diameter of 100 nm) without PIL cores as the control experiment. Under the same conditions, the loading efficiency of mesoporous silica nanoparticles was no larger

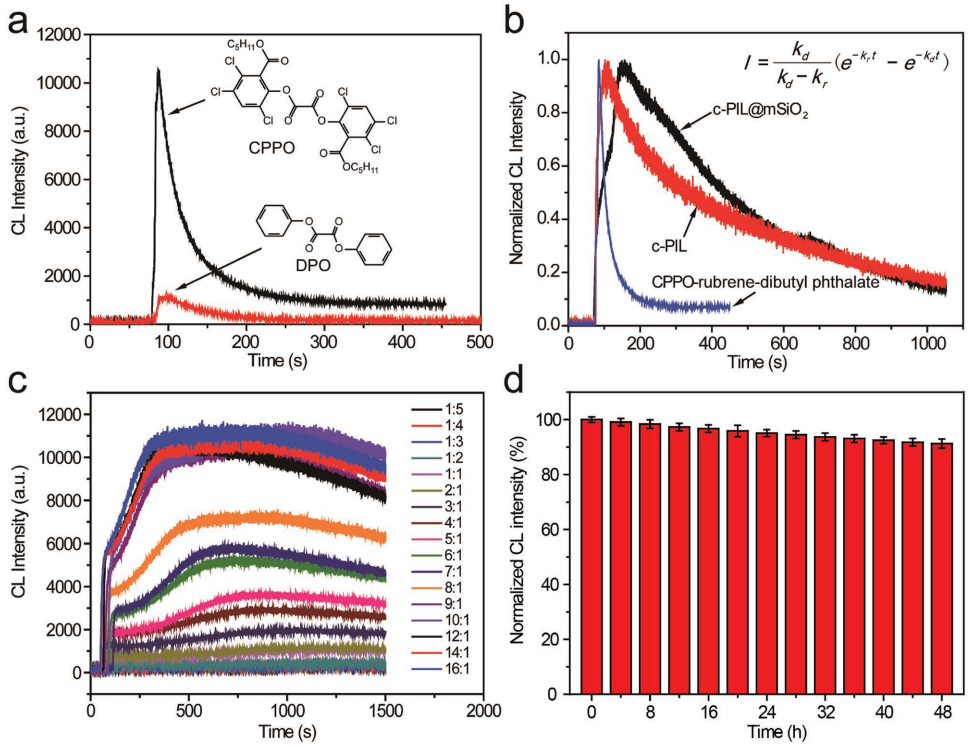

Figure 2. a) Comparison of the CL efficient of CPPO and DPO in dibutylphthalate. The H_2O_2 (25 µL, 10^{-5} M) were injected into CPPO (200 µL, 10^{-4} M, contain 10^{-5} M rubrene) and DPO (200 µL, 10^{-4} M, contain 10^{-5} M rubrene) in dibutylphthalate solution respectively. b) CL kinetic profiles of CPPO + rubrene loaded in dibutylphthalate, PIL nanoparticles and PIL@$mSiO_2$ nanoparticles. The kinetic parameters were determined with nonlinear fitting according to the given equation, where I is the normalized CL intensity. k_r and k_d are the rate constants for rising and decay, respectively. c) CL curves of PIL@$mSiO_2$ nanoparticles loaded CPPO/rubrene with different molar ratios from 1:5 to 16:1. d) The stability of c-PIL@$mSiO_2$ after dispersion in PBS.

than 2.1%, indicating the importance of PIL cores for PO-CL reagents resevation. In addtion, the release profile (Figure S6, Supporting Information) showed negligible release of PO-CL regents in PIL@$mSiO_2$. As shown in **Figure 2**a, one order of magnitude enhancement of CL signal was achieved in response to the same H_2O_2 concentration by using CPPO than that of diphenyloxalate (DPO). The results indicate that previously reported DPO polymers-based CL nanoprobes sacrificed H_2O_2 sensitivity.[10a,12,19] The CL dynamics of PO-CL reagents in dibutylphthalate, and c-PILs and c-PIL@$mSiO_2$ in PBS were then investigated and compared. As shown in Figure 2b, both c-PILs and c-PIL@$mSiO_2$ response to H_2O_2 sensitively, and their CL life time was prolonged 3 (k_d = 0.149 s^{-1}) and 13 (k_d = 0.037 s^{-1}) times respectively in comparison with that of PO-CL reagents in dibutylphthalate (k_d = 0.484 s^{-1}). The longer CL life time is benifical to imaging analysis. As shown in Figure 2c, c-PIL@$mSiO_2$ loaded with CPPO and rubrene of different molar ratios from 1:5 to 16:1 showed different CL characters in 10 µm H_2O_2 PBS. The molar ratio of 10:1 were employed in following unless otherwise noted. The storage stability of c-PIL@$mSiO_2$ under physiological conditions was investigated by monitoring CL intensity every 4 h after dispersion in PBS. The CL intensity lost less than 8% after contact with water over 48 h (Figure 2d), suggesting that the c-PIL@$mSiO_2$ can preserve the hydrolysis of CPPO. This is important to accurate and robust detection.

After the investigation of CL dynamics of c-PIL@$mSiO_2$, we further explored its steady-state CL properties. The CL spectrum of c-PIL@$mSiO_2$ measured by a fluorescence spectrometer with a maximum peak at 560 nm, which is similar to the fluorescent spectrum of rubrene (**Figure 3**a). The CL intensity is strong enough to be visible under dark (inset of Figure 3a). The response selectivity of c-PIL@$mSiO_2$ to H_2O_2 over other competing cellular ROS like hypochlorite (OCl^-), superoxide ($O_2•^-$) and hydroxyl radical (•OH) and reactive nitrogen species was investigated (Figure 3b). The selectivity over the competing ROS was higher than 20 times, which is high enough for selective detection of H_2O_2. The quantitative CL response of c-PIL@$mSiO_2$ to different concentrations of H_2O_2 was subsequently studied in PBS for simulating physiological conditions. As shown in Figure 3c,d, the CL intensity increased steadily with increasing H_2O_2 concentrations. The plot of CL intensity versus the H_2O_2 concentration gives a linear in the range of 10^{-9}–10^{-7} M. The c-PIL@$mSiO_2$ was capable of detecting H_2O_2 at concentrations as low as 5×10^{-9} M. This detection limit is lower than the normal H_2O_2 concentration intracellular and in vivo,[20] and is significantly better than that of the DPO polymer-based CL nanoprobes (250×10^{-9} M),[10a] CL micelles (100×10^{-9} M),[19] and that of fluorescent probes (≈100×10^{-9} M).[21] The improved sensitivity of the c-PIL@$mSiO_2$ should be due to the high CL efficiency of CPPO and the unique structural properties of PIL.

As cytotoxicity is one of the critical concerns in development of biomaterials, the cytotoxicity of c-PIL@$mSiO_2$ was evaluated by 3-(4,5-dimethylthiazol-2-yl)-2,5-diphenyltetrazolium bromide (MTT) assay. The c-PIL@$mSiO_2$ showed negligible cytotoxicity

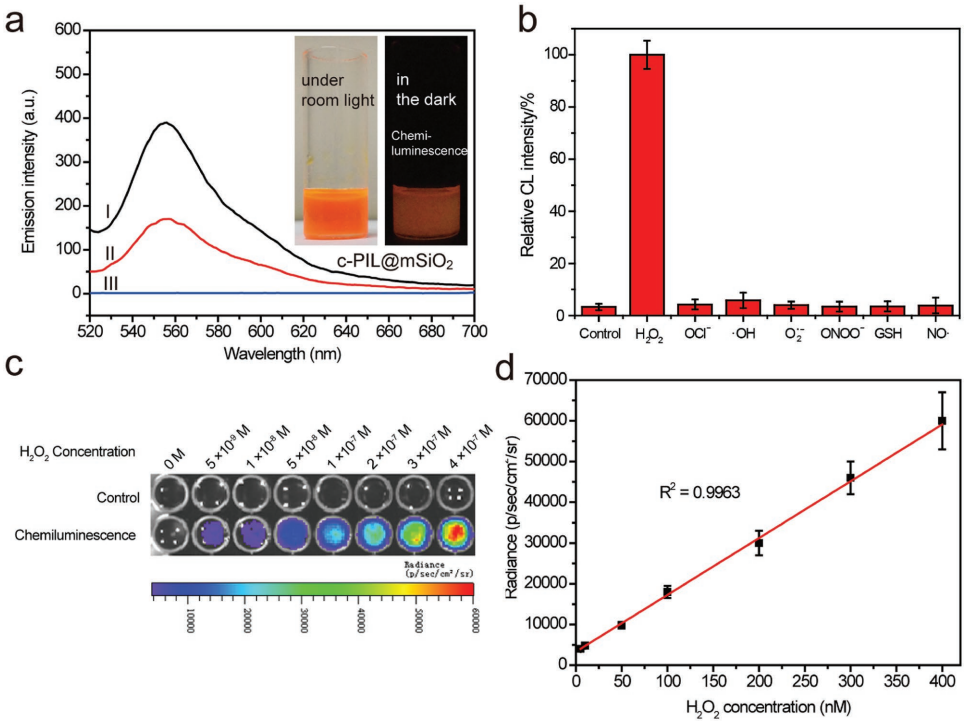

Figure 3. a) Fluorescent and CL spectra of c-PIL@mSiO$_2$ (I, II), the emission spectra of c-PIL@mSiO$_2$ before injected H_2O_2 (III); inset: Photographs of the generated CL of c-PIL@mSiO$_2$ under room light and in the dark. b) CL response of c-PIL@mSiO$_2$ (300 μg mL^{-1}) to various reactive oxygen species at 10×10^{-6} M. Mean ± s.d., $n = 3$. H_2O_2, OCl^-, $O_2^{\bullet -}$, $ONOO^-$, and GSH solutions were prepared by directly diluting commercially available H_2O_2, NaOCl, KO_2, NaONOO, and GSH respectively. •OH was generated from Fenton reaction between Fe^{2+} and H_2O_2. NO• was generated from diethylamine NONOate. c) CL images of c-PIL@mSiO$_2$ in the presence of low-level H_2O_2 captured with IVIS-200 imaging system. d) A correlation between the amount of H_2O_2 and the CL intensity, estimated from (c) in triplicate.

at concentration up to 800 μg mL^{-1} for RAW264.7 macrophages (Figure S7, Supporting Information). The results demonstrate that c-PIL@mSiO$_2$ have excellent biocompatibility in vitro and great potential for bioimaging applications.

The intracellular H_2O_2 CL detection with c-PIL@mSiO$_2$ was then carried out by using a model cell line, RAW264.7 macrophages. The cell permeability of c-PIL@mSiO$_2$ was first confirmed by 3D confocal fluorescence microscopy (CFM). Under light excitation, the c-PIL@mSiO$_2$ can emit red fluorescence of the loaded rubrene allowing for tracing of the spatial position of c-PIL@mSiO$_2$. RAW264.7 cells incubated with c-PIL@mSiO$_2$ displayed fluorescence signals of rubrene (**Figure 4**a, *x*–*y* plane). The 3D CFM images in the *x*–*z* and *y*–*z* planes clearly showed the c-PIL@mSiO$_2$ inside the cell, but not on the surface or outside (Figure 4a, bottom and right panels). This indicates that the c-PIL@mSiO$_2$ are taken up by cells avidly to allow for intracellular H_2O_2 imaging. RAW264.7 macrophages are known to produce micromolar levels of intracellular H_2O_2 upon stimulation with phorbol myristate acetate (PMA).[22] As shown in Figure 4b, significant CL signals were only observed from the sample wells containing RAW264.7 cells labeled with c-PIL@mSiO$_2$. Upon stimulation with PMA to induce an immune response, a significant CL signal was observed due to increased intracellular level (group 1). Even without immune stimulation, the labeled cells showed noticeable CL signal (group 5), implying that the enhanced CL from c-PIL@mSiO$_2$ can sensitively detect the low level endogenous H_2O_2 under normal physiological conditions. To ensure the collected CL signals were intracellular, the cells were washed with a cell-impermeable H_2O_2 scavenger, catalase, solution before assays.

The in vivo imaging of c-PIL@mSiO$_2$ toward H_2O_2 in deep tissues of mice was assessed by an IVIS-200 imaging system without using photoexcitation. A suspension of c-PIL@mSiO$_2$ in the absence or presence of H_2O_2 was injected intramuscularly at a depth of about 3 mm. **Figure 5**a,b demonstrate that c-PIL@mSiO$_2$ can provide a great image contrast between the presence and absence of H_2O_2. For example, a CL intensity of 250 000 p s^{-1} cm^{-2} sr^{-1} was observed from the particles injected with 10 nmol H_2O_2 (IV), whereas a peak emission intensity of only 60 000 p s^{-1} cm^{-2} sr^{-1} was detected from particles injected with 1 nmol H_2O_2 (II) and much lower emission intensity (20 000 p s^{-1} cm^{-2} sr^{-1}) was observed from the particles without H_2O_2 (III).

Furthermore, the ability of the c-PIL@mSiO$_2$ to image endogenously produced H_2O_2 in mice is investigated using a mice model of lipopolysaccharide (LPS) induced acute inflammation. The overproduction of H_2O_2 is implicated in numerous inflammatory diseases, such as atherosclerosis, liver hepatitis and chronic obstructive pulmonary disease.[23] Therefore, there is a great interest in imaging H_2O_2 in vivo to act as a diagnostic for inflammatory diseases. Acute inflammation in ankle joints of mice was induced by intra-articular injection of LPS, and 48 h later (an early stage of inflammation),[24] c-PIL@mSiO$_2$ was also injected into

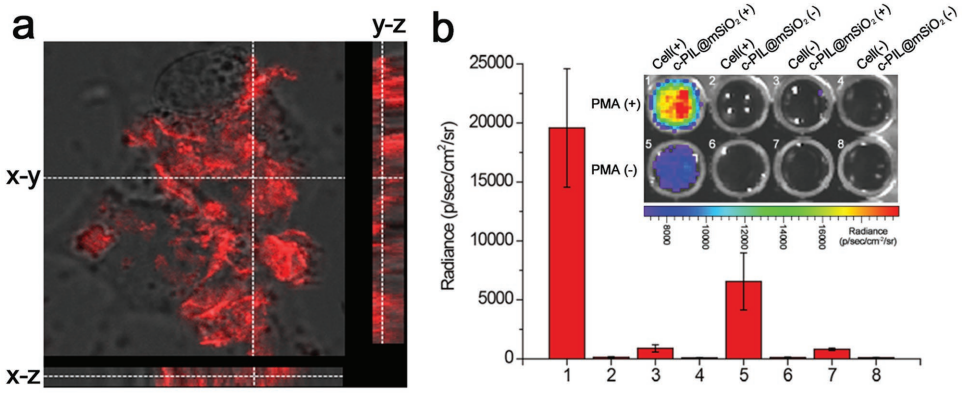

Figure 4. a) Confocal laser-scanning images along the *z*-axis of RAW 264.7 cells loaded with 300 μg mL^{-1} c-PIL@mSiO$_2$ in serum-free medium for 10 min. b) Representative image (inset) and quantification of CL emission intensity from experimental groups 1–8 (mean ± s.d., $n = 5$) with or without nanoparticles, cells, and PMA stimulation, estimated from the inset.

the inflammatory site and CL imaged in an IVIS imaging system with 1 min of acquisition time. Figure 5c shows a representative image of CL emitted from mice treated with LPS. The LPS-treated site (right ankle joint) showed a peak emission intensity of 100 000 p s^{-1} cm^{-2} sr^{-1} from the right ankle joint; while weak CL emission was detected at the left ankle joint which was not given LPS, demonstrating that the c-PIL@mSiO$_2$ can image H_2O_2 in vivo during inflammatory responses. Figure 5d demonstrates that the right ankle joint of mice treated with LPS and c-PIL@mSiO$_2$ generated almost six times higher CL intensity than the left ankle joint of mice treated with saline and c-PIL@mSiO$_2$. These results suggest that c-PIL@mSiO$_2$ have the potential for imaging H_2O_2 associated inflammatory diseases.

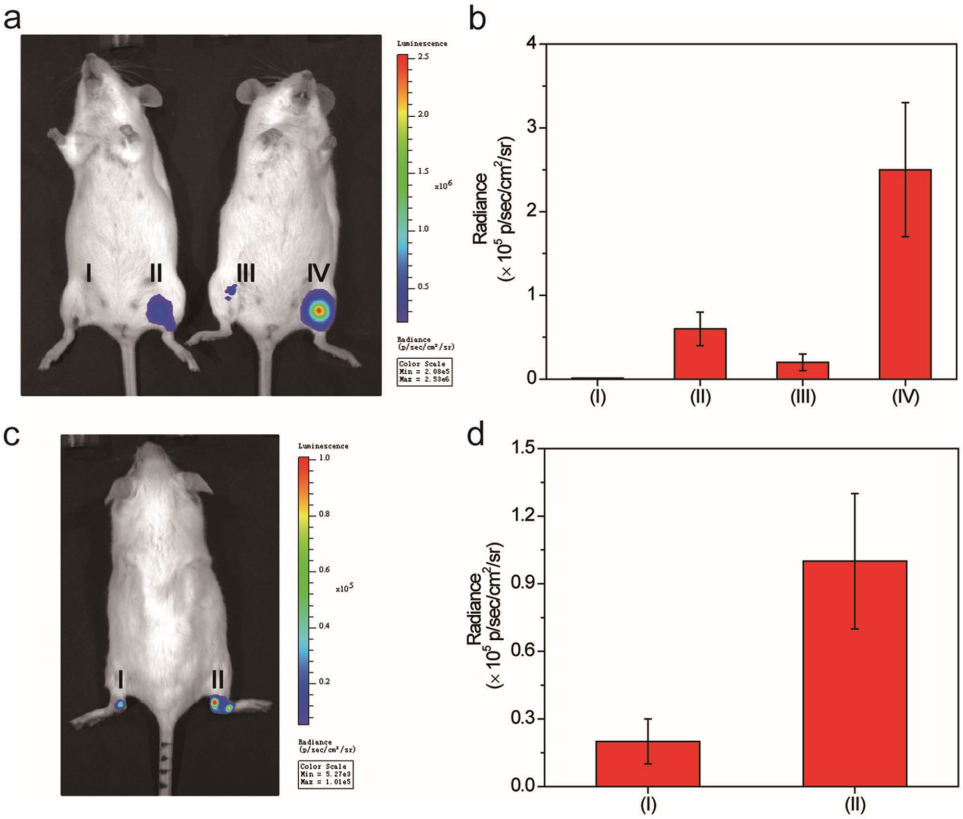

Figure 5. a) In vivo imaging of exogenous H_2O_2 using c-PIL@mSiO$_2$. (I) negative control; (II) c-PIL@mSiO$_2$ + 1 nmol of H_2O_2; (III) c-PIL@mSiO$_2$ only; (IV) c-PIL@mSiO$_2$ + 10 nmol of H_2O_2. b) Quantification of CL emission intensity of groups (I–IV) estimated from (a), mean ± s.d., $n = 3$. c) In vivo CL imaging of the LPS-induced arthritis mice model using c-PIL@mSiO$_2$. (I) pre-injected PBS + c-PIL@mSiO$_2$, (II) pre-injected LPS + c-PIL@mSiO$_2$. d) Quantification of CL emission intensity of groups (I) and (II) estimated from (a), mean ± s.d., $n = 3$.

3. Conclusion

In summary, we describe a highly sensitive and selective H_2O_2 CL imaging nanoprobe c-PIL@mSiO_2, which composes of a PIL core and a hydrophilic mesoporous silica shell. The H_2O_2 detection sensitivity of c-PIL@mSiO_2 was nM level which is much better than many previously reported fluorescent and luminescent probes. Without external light source, this nanoprobe was successfully applied in live mice to selectively visualize H_2O_2 in normal and inflammation tissues. More importantly, the c-PIL@mSiO_2 detects intracellular H_2O_2 without cell cytolysis via CL signal for the first time. The above breakthroughs achieved are attributed to several remarkable advantages of the new c-PIL@mSiO_2 nanoprobe: (1) the extraordinary properties of the PIL core, such as constructed by multiple alternating hydrophilic and hydrophobic nanodomains, swelling in organic solvents and self-adaptive ability offers facilitation for loading PO-CL reagents with high CL reactivity, (2) the use of CPPO greatly elevates the CL intensity, (3) the mesoporous silica shell makes the nanoprobe biocompatible, dispersible, and cell-penetrable, (4) greatly improved sensitivity should also owing to red luminescence, longer CL time and no background fluorescence interference without external excitation source. This nanoprobe should have great potential as a diagnostic reagent for H_2O_2-associated diseases. And also, we can use the core–shell PIL@mSiO_2 structure to CL detection of other active molecules intracellular and in vivo.

4. Experimental Section

Materials, analytical instrumentation, synthetic procedures, and additional experimental data are provided in the Supporting Information.

Preparation of c-PIL@mSiO_2: CPPO (67.7 mg, 0.1 mmol) and rubrene (5.4 mg, 0.01 mmol) were added to 2 mL of acetone, and the mixture was stirred for 10 min, until a homogeneous red solution. The PIL@mSiO_2 (100 mg) was added, and the mixture was then stirred at room temperature for 24 h. The nanoparticles were then collected by 13 000 rpm centrifugation. The supernatant was decanted. The remaining acetone was removed by rotary evaporation. The product was dried in vacuum at 40 °C as an orange-red solid.

H_2O_2 Quantification: An aqueous solution of c-PIL@mSiO_2 (100 µL, 300 µg mL^{-1}) was transferred to black 96-well plates. H_2O_2 solutions with different concentrations were prepared by diluting the stock H_2O_2 solution (10^{-6} M). The solution CL intensities were measured by IVIS-200 imaging system with 1 min acquisition. The CL response of c-PIL@mSiO_2 (300 µg mL^{-1}) to various reactive oxygen species were evaluated at 10^{-5} M. OCl^- and $O_2^{\bullet -}$ solutions were prepared by directly diluting commercially available NaOCl and KO_2, respectively. ·OH was generated by reacting Fe^{2+} with H_2O_2.

Intracellular Labeling and Imaging: RAW264.7 macrophages were cultured in DMEM with 10% FBS, 0.1% streptomycin and 0.1% penicillin in a humidified 5% CO_2 incubator at 37 °C. Prior to experiments, cells were rinsed twice with PBS to remove the remnant growth medium and then incubated in a serum-free medium (1.8 mL) containing c-PIL@mSiO_2 (300 µg mL^{-1}) for 10 min. For photoluminescence imaging, RAW264.7 macrophages were seeded onto confocal dish and then washed twice with PBS and imaged using a confocal laser scanning microscope (OLYMPUS, Japan). For CL imaging, cells were seeded onto black 96-well plates and pretreated for 1 h in a serum-free medium (1.8 mL) containing 200 µL of PMA (20 µg) to induce immune response or 200 µL of PBS for a normal control. The pretreated cells were labeled with c-PIL@mSiO_2 (300 µg mL^{-1}) for 10 min and then imaged with an IVIS Spectrum imaging system (Caliper, USA) with 1 min acquisition.

In Vivo Imaging of Exogenous H_2O_2: KM mice (female, 6 weeks of age) were anaesthetized using 2% of diethyl ether in oxygen. c-PIL@mSiO_2 (10 mg mL^{-1} in 0.1 M sodium phosphate buffer, pH 7.4) were mixed with either 1 or 10 µL of a 1×10^{-3} M H_2O_2 solution (pH 7.4), and 50 µL of the nanoparticle suspension was injected intramuscularly into the legs of anaesthetized mice. CL images were captured with a 1 min acquisition time using an IVIS imaging system (Caliper, USA).

In Vivo Imaging of Endogenous H_2O_2: Acute inflammation was induced by intra-articular injection of LPS (20 µL, 5 mg mL^{-1} in PBS; or 20 µL of PBS alone for a normal control) into the ankle of mice. After 48 h LPS treatment, c-PIL@mSiO_2 (50 µL, 10 mg mL^{-1}) was intra-articularly administered into mice ankle with or without LPS treatment. In vivo CL imaging was conducted with an IVIS Spectrum imaging system with 1 min acquisition.

Supporting Information

Supporting Information is available from the Wiley Online Library or from the author.

Acknowledgements

This work was financially supported by the National Natural Science Foundation of China (No. 21675016), Chongqing Basic and Frontier Research Program (No. cstc2016jcyjA0328), and the 100 Young Plan by Chongqing University (No. 0236011104410).

Conflict of Interest

The authors declare no conflict of interest.

Keywords

chemiluminescence, hydrogen peroxide, intracellular detection, nanoprobes, poly (ionic liquid)

Received: September 7, 2017
Revised: November 14, 2017
Published online: January 15, 2018

[1] C. N. Morrell, *Circ. Res.* **2008**, *103*, 571.
[2] A. Boveris, N. Oshino, B. Chance, *Biochem. J.* **1972**, *128*, 617.
[3] a) M. Giorgio, M. Trinei, E. Migliaccio, P. G. Pelicci, *Nat. Rev. Mol. Cell Biol.* **2007**, *8*, 722; b) Y. Huang, L. Mucke, *Cell* **2012**, *148*, 1204; c) K. Zhang, R. J. Kaufman, *Nature* **2008**, *454*, 455.
[4] P. Wardman, *Free Radical Biol. Med.* **2007**, *43*, 995.
[5] a) M. Onoda, S. Uchiyama, A. Endo, H. Tokuyama, T. Santa, K. Imai, *Org. Lett.* **2003**, *5*, 1459; b) Y. Yang, Q. Zhao, W. Feng, F. Li, *Chem. Rev.* **2013**, *113*, 192; c) H. Zeng, W. Qiu, L. Zhang, R. Liang, J. Qiu, *Anal. Chem.* **2016**, *88*, 6342.
[6] L. Yang, N. Li, W. Pan, Z. Yu, B. Tang, *Anal. Chem.* **2015**, *87*, 3678.
[7] C. Dodeigne, L. Thunus, R. Lejeune, *Talanta* **2000**, *51*, 415.
[8] a) G. C. V. Bittner, E. A. Dubikovskaya, C. R. Bertozzi, C. J. Chang, *Proc. Natl. Acad. Sci. USA* **2010**, *107*, 21316; b) R. Kojima, H. Takakura, M. Kamiya, E. Kobayashi, T. Komatsu, T. Ueno, T. Terai, K. Hanaoka, T. Nagano, Y. Urano, *Angew. Chem., Int. Ed.* **2015**, *54*, 14768; c) G. C. V. Bittner, C. R. Bertozzi, C. J. Chang, *J. Am. Chem. Soc.* **2013**, *135*, 1783.
[9] a) M. Khalid, S. P. S. Jr., L. F. M. L. Ciscato, F. H. Bartoloni, W. J. Baader, *Photochem. Photobiol. Sci.* **2015**, *14*, 1296;

b) S. P. S. Jr., M. Khalid, F. A. Augusto, W. J. Baader, *J. Photochem. Photobiol. A* **2016**, *321*, 143.

[10] a) D. Lee, S. Khaja, J. C. V. Castano, M. Dasari, C. Sun, J. Petros, W. R. Taylor, N. Murthy, *Nat. Mater.* **2007**, *6*, 765; b) S. Cho, O. Hwang, I. Lee, G. Lee, D. Yoo, G. Khang, P. M. Kang, D. Lee, *Adv. Funct. Mater.* **2012**, *22*, 4038.

[11] a) D. Lee, V. R. Erigala, M. Dasari, J. Yu, R. M. Dickson, N. Murthy, *Int. J. Nanomed.* **2008**, *3*, 471; b) J. Geng, K. Li, W. Qin, B. Z. Tang, B. Liu, *Part. Part. Syst. Char.* **2014**, *31*, 1238; c) A. Singh, Y. H. Seo, C.-K. Lim, J. Koh, W.-D. Jang, I. C. Kwon, S. Kim, *ACS Nano* **2015**, *9*, 9906.

[12] D. Lee, S. Bae, Q. Ke, J. Lee, B. Song, S. A. Karumanchi, G. Khang, H. S. Choi, P. M. Kang, *J. Controlled Release* **2013**, *172*, 1102.

[13] V. S. Lin, B. C. Dickinson, C. J. Chang, *Methods Enzymol.* **2013**, *526*, 19.

[14] a) Y. Yang, M. Ambrogi, H. Kirmse, Y. Men, M. Antonietti, J. Yuan, *Chem. Mater.* **2015**, *27*, 127; b) J. Yuan, S. Soll, M. Drechsler, A. H. E. Muller, M. Antonietti, *J. Am. Chem. Soc.* **2011**, *133*, 17556.

[15] M. Koebe, M. Drechsler, J. Weber, J. Yuan, *Macromol. Rapid Commun.* **2012**, *33*, 646.

[16] a) Y. Deng, D. Qi, C. Deng, X. Zhang, D. Zhao, *J. Am. Chem. Soc.* **2008**, *130*, 28; b) J. Chen, S. Lei, K. Zeng, M. Wang, A. Asif, X. Ge, *Nano Res.* **2017**, *10*, 2351; c) C. Li, P. Wang, Y. Tian, X. Xu, H. Hou, M. Wang, G. Qi, Y. Jin, *ACS Catal.* **2017**, *7*, 5391; d) Y. Li, C. Jin, G. Yuan, J. Han, M. Wang, R. Guo, *Langmuir* **2017**, *33*, 7486; e) M. You, S. Yang, W. Tang, F. Zhang, P. He, *ACS Appl. Mater. Interfaces* **2017**, *9*, 13855.

[17] J. Wang, X. Li, S. Zhang, R. Lu, *Nanoscale* **2013**, *5*, 4823.

[18] a) Z. Chen, J. Wang, Z. Lin, G. Chen, *Talanta* **2007**, *72*, 1410; b) F. J. Alvarez, N. J. Parekh, B. Matuszewski, R. S. Givens, T. Higuchi, R. L. Schowen, *J. Am. Chem. Soc.* **1986**, *108*, 6435.

[19] M. Dasari, D. Lee, V. R. Erigala, N. Murthy, *J. Biomed. Mater. Res. A* **2009**, *89A*, 561.

[20] a) S. G. Rhee, *Science* **2006**, *312*, 1882; b) T. Strowig, J. H. Mejia, E. Elinav, R. Flavell, *Nature* **2012**, *481*, 278; c) Z. Li, T. Liang, S. Lv, Q. Zhuang, Z. Liu, *J. Am. Chem. Soc.* **2015**, *137*, 11179.

[21] a) M. C. Y. Chang, A. Pralle, E. Y. Isacoff, C. J. Chang, *J. Am. Chem. Soc.* **2004**, *126*, 15392; b) H. Maeda, Y. Fukuyasu, S. Yoshida, M. Fukuda, K. Saeki, H. Matsuno, Y. Yamauchi, K. Yoshida, K. Hirata, K. Miyamoto, *Angew. Chem., Int. Ed.* **2004**, *43*, 2389.

[22] H. Li, Q. Li, X. Wang, K. Xu, Z. Chen, X. Gong, X. Liu, L. Tong, B. Tang, *Anal. Chem.* **2009**, *81*, 2193.

[23] a) C. Polytarchou, M. Hatziapostolou, E. Papadimitriou, *J. Biol. Chem.* **2005**, *280*, 40428; b) A. Laurent, C. Nicco, C. Chereau, C. Goulvestre, J. Alexandre, A. Alves, E. Levy, F. Goldwasser, Y. Panis, O. Soubrane, B. Weill, F. Batteux, *Cancer Res.* **2005**, *65*, 948; c) J. L. Hirpara, M. V. Clement, S. Pervaiz, *J. Biol. Chem.* **2001**, *276*, 514.

[24] W. T. Chen, U. Mahmood, R. Weissleder, C. H. Tung, *Arthritis Res. Ther.* **2005**, *7*, R310.

